Title

Limited oxygen production in the Mesoarchean ocean

Journal

Proceedings of the National Academy of Sciences of the United States of America, 116(14)

ISSN

0027-8424

Authors

Ossa, Frantz Ossa
Hofmann, Axel
Spangenberg, Jorge E
et al.

Publication Date

2019-04-02

DOI

10.1073/pnas.1818762116

Peer reviewed

Limited oxygen production in the Mesoarchean ocean

Frantz Ossa Ossa[a,b,1], Axel Hofmann[b], Jorge E. Spangenberg[c], Simon W. Poulton[d], Eva E. Stüeken[e], Ronny Schoenberg[a], Benjamin Eickmann[a,b], Martin Wille[f], Mike Butler[g], and Andrey Bekker[b,h]

[a]Department of Geosciences, University of Tuebingen, 72074 Tuebingen, Germany; [b]Department of Geology, University of Johannesburg, 2092 Johannesburg, South Africa; [c]Institute of Earth Surface Dynamics, University of Lausanne, 1015 Lausanne, Switzerland; [d]School of Earth and Environment, University of Leeds, Leeds LS2 9JT, United Kingdom; [e]School of Earth & Environmental Sciences, University of St. Andrews, St. Andrews KY16 9AL, United Kingdom; [f]Institute of Geological Sciences, University of Bern, 3012 Bern, Switzerland; [g]Environmental Isotope Laboratory, IThemba LABS, 2050 Johannesburg, South Africa; and [h]Department of Earth Sciences, University of California, Riverside, CA 92521

Edited by Mark H. Thiemens, University of California, San Diego, La Jolla, CA, and approved February 28, 2019 (received for review October 31, 2018)

The Archean Eon was a time of predominantly anoxic Earth surface conditions, where anaerobic processes controlled bioessential element cycles. In contrast to "oxygen oases" well documented for the Neoarchean [2.8 to 2.5 billion years ago (Ga)], the magnitude, spatial extent, and underlying causes of possible Mesoarchean (3.2 to 2.8 Ga) surface-ocean oxygenation remain controversial. Here, we report $\delta^{15}N$ and $\delta^{13}C$ values coupled with local seawater redox data for Mesoarchean shales of the Mozaan Group (Pongola Supergroup, South Africa) that were deposited during an episode of enhanced Mn (oxyhydr)oxide precipitation between ∼2.95 and 2.85 Ga. Iron and Mn redox systematics are consistent with an oxygen oasis in the Mesoarchean anoxic ocean, but $\delta^{15}N$ data indicate a Mo-based diazotrophic biosphere with no compelling evidence for a significant aerobic nitrogen cycle. We propose that in contrast to the Neoarchean, dissolved O_2 levels were either too low or too limited in extent to develop a large and stable nitrate reservoir in the Mesoarchean ocean. Since biological N_2 fixation was evidently active in this environment, the growth and proliferation of O_2-producing organisms were likely suppressed by nutrients other than nitrogen (e.g., phosphorus), which would have limited the expansion of oxygenated conditions during the Mesoarchean.

oxygen oasis | nitrogen isotopes | nutrient limitation | oxygenic photosynthesis | Mesoarchean

A dramatic rise in atmospheric oxygen level during the Great Oxidation Event (GOE) at ∼2.4 billion years ago (Ga) is marked by the disappearance of mass-independent fractionation of sulfur isotopes, oxidation of detrital pyrite and uraninite, and the appearance of red beds, reflecting the irreversible transition from an anoxic to an oxic world (1, 2). While it is widely accepted that oxygenic photosynthesis was a first-order control on the GOE (3), Archean shallow-marine "oxygen oases" and "whiffs" of atmospheric oxygen (O_2) have been proposed to have occurred up to several hundred million years before the GOE (4–18). However, while processes that drove oxygen production during transient and localized oxygenation events in the Neoarchean (2.8 to 2.5 Ga) are supported by a wide range of geochemical proxies (e.g., refs. 4–6 and 13–18), those from the Mesoarchean (3.2 to 2.8 Ga) are constrained by only a limited number of studies (7–12).

The nitrogen (N) cycle from the Paleoarchean up to ∼2.7 Ga is widely considered to have been dominated by bioavailable ammonia (NH_4^+) under anoxic water-column conditions (15, 16). Oxidation of NH_4^+ would have been suppressed in an early Archean ocean characterized by extremely low O_2 concentrations (15–17). Free O_2 is produced through oxygenic photosynthesis, the rate of which is mainly controlled by the concentrations of bioavailable N and phosphorus (P) (19–24). While the sedimentary $\delta^{15}N$ record suggests that N was bioavailable and that diazotrophic molybdenum (Mo)-based nitrogenase dominated N_2 fixation in the Mesoarchean, the record also places a robust minimum age for the occurrence of aerobic N cycling at ∼2.72 Ga in the Neoarchean (e.g., refs. 15 and references therein). Indeed, prominent N isotope excursions in the Neoarchean provide evidence for temporary NH_4^+ oxidation, and thus the $\delta^{15}N$ record has been used to infer the development of locally oxygenated surface-ocean environments after ∼2.7 Ga (5, 15, 17, 18, 25).

Independently, stable-isotope systematics of redox-sensitive elements such as iron (Fe), Mo, uranium, and sulfur, as well as locally enhanced manganese (Mn) (oxyhydr)oxide precipitation, support an earlier emergence of oxygenic photosynthesis and episodic development of oxygen oases in the Mesoarchean surface ocean (7–9, 11), well before currently accepted evidence for oxidative nitrogen cycling. Furthermore, phylogenomic estimates based on molecular clocks also suggest that cyanobacterial stems capable of oxygenic photosynthesis might find their roots in the Archean, with a development and progressive diversification starting as early as ∼3.5 Ga (26–28). However, the factors that caused a delay in pervasive oxygenation of the atmosphere–hydrosphere system after the establishment of oxygenic photosynthesis earlier in the Archean remain poorly constrained, particularly with regard to the role of their two main biolimiting nutrients, N and P (19–23). Modeling studies have demonstrated that low dissolved P concentrations would severely suppress the rate of oxygenic photosynthesis and ultimately the spatial extent of Archean oxygen oases (29). However, there is currently no consensus on dissolved P concentrations in the Archean ocean (21–23, 30–32).

To assess controls on the spatial development and intensity of Earth's first oxygen oases, we measured nitrogen ($\delta^{15}N$) and

Significance

Episodic development of "oxygen oases" during the Archean Eon characterizes the hundreds of millions of years transition to permanent oxygenation in the atmosphere–hydrosphere system at the Great Oxidation Event (∼2.4–2.3 Ga). One of these well-characterized oxygen oases is recorded in Mesoarchean sediments of the Pongola Supergroup. We show that in contrast to the Neoarchean, biological oxygen production in a shallow ocean having Mo-based nitrogen fixation was not sufficient to result in a dissolved nitrogen reservoir that would carry the isotopic effects of an aerobic nitrogen cycle. Nevertheless, it appears that low concentrations of bioavailable phosphorus, rather than nitrogen, suppressed the growth and expansion of oxygenic photosynthesizers and may explain why pervasive and permanent oxygenation was delayed during the Archean Eon.

Author contributions: F.O.O., A.H., R.S., and A.B. designed research; F.O.O., A.H., and A.B. performed research; F.O.O. contributed new reagents/analytic tools; F.O.O., A.H., J.E.S., S.W.P., E.E.S., M.B., and A.B. analyzed data; and F.O.O., A.H., J.E.S., S.W.P., E.E.S., R.S., B.E., M.W., M.B., and A.B. wrote the paper.

The authors declare no conflict of interest.

This article is a PNAS Direct Submission.

[1]To whom correspondence should be addressed. Email: frantz.ossaossa@gmail.com.

This article contains supporting information online at www.pnas.org/lookup/suppl/doi:10.1073/pnas.1818762116/-/DCSupplemental.

Published online March 20, 2019.

organic carbon ($\delta^{13}C_{org}$) isotopes, local water-column redox proxies (Fe speciation and Mn concentrations), and elemental data for shales of the ~2.95- to 2.85-Ga Mozaan Group, Pongola Supergroup, South Africa (*SI Appendix* includes geologic setting and all data). Our aim is to clarify the factors that controlled the nature and development of oxygen oases in the Mesoarchean.

Results and Discussion

Water Column Redox Reconstruction. Our samples span from a shallow-marine (above wave base) depositional setting in the White Mfolozi Inlier to a deeper-water (below wave base) equivalent in the Nongoma area and comprise three sequences deposited at different water depths (Fig. 1 and *SI Appendix*, Figs. S1 and S2 and Table S1). In the White Mfolozi Inlier, sequence I, deposited in the most proximal, intertidal to shallow subtidal setting, is characterized by high Mn contents and Mn/Fe ratios compared with average values for shales of the Pongola Supergroup (ref. 33 and *SI Appendix*, Table S1). It has mostly high ratios of highly reactive Fe to total Fe (FeHR/FeT), and high Fe/Al ratios (see *SI Appendix*, *Methods* for detailed analytical techniques). Sequence II was deposited in a deep subtidal but above fair-weather wave base setting and shows a progressive decrease in Mn contents and Mn/Fe, FeHR/FeT, and Fe/Al ratios, whereas Mn and Fe contents are higher than those in average Pongola shales (ref. 33 and *SI Appendix*, Table S1). The uppermost sequence III represents deepening to between fair-weather and storm wave base and is characterized by persistently low Mn contents and Mn/Fe, FeHR/FeT, and Fe/Al ratios, with Mn and Fe contents similar to those in average Pongola shales (ref. 33 and *SI Appendix*, Table S1). In the more distal, deeper-water setting of the Nongoma area, where distinct compositional trends were not observed, Fe/Al ratios tend to be high, but Mn contents remain low and Mn/Fe ratios shift to values lower than the average for shales of the Pongola Supergroup (ref. 33 and *SI Appendix*, Table S1).

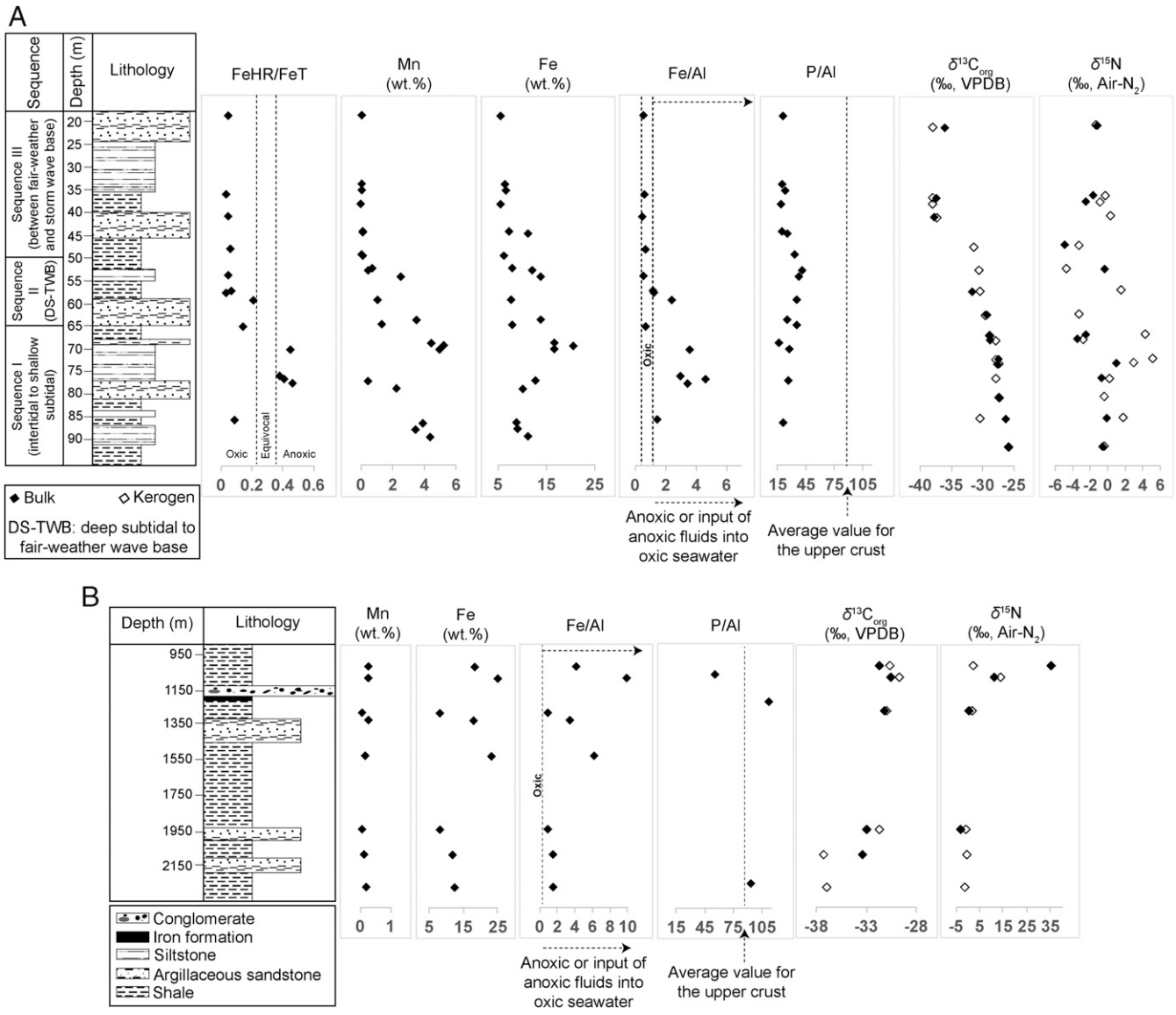

Fig. 1. Geochemical data for shale samples plotted along the lithostratigraphic columns of the studied sections of the Mozaan Group (Pongola basin) from the shallow part of the Ntombe Formation in the White Mfolozi Inlier (*A*), and its deeper-water equivalent in the Nongoma area (*B*) (see *SI Appendix*, Fig. S2 for details). Sequences are defined based on water-depth indicators and chemostratigraphic data. Vertical lines and horizontal arrows on Fe/Al plots are based on the description provided in *SI Appendix*, *Supplementary Methods* and on the data in *SI Appendix*, Table S1 (70), whereas the average value for the upper crust on P/Al plots is from ref. 65.

To explain these data, we invoke upwelling of anoxic waters that were rich in Fe^{2+} and Mn^{2+} into oxic shallow waters. Precipitation of Fe as (oxyhydr)oxide minerals may have started under low-oxygen or anoxic conditions, potentially via photoferrotrophy in shallower waters directly overlying deeper anoxic waters (34), and this likely explains the observed Fe enrichments in the distal Nongoma setting (Fig. 1*B*). Fe(II) oxidation would have been progressive during upwelling, leading to increased FeHR/FeT and Fe/Al enrichments (Fig. 1*A*) as water depth shallowed through a redoxcline (as captured by sequence II in the White Mfolozi Inlier) into the shallow and locally oxygenated waters of sequence I, where Mn(IV) (oxyhydr)oxides precipitated (Figs. 1*A* and 2). Increased Mn/Fe ratios in shallower waters thus reflect progressive removal of dissolved Fe(II) and/or enhanced precipitation of Mn (oxyhydr)oxides as upwelling anoxic waters reached the redox threshold for Mn(II) oxidation. However, sequence III in the White Mfolozi Inlier has Mn/Fe ratios similar to the average value for shales of the Pongola Supergroup, with no evidence for FeHR enrichment, likely reflecting deeper anoxic waters where there was limited oxidant availability to promote Fe or Mn (oxyhydr)oxide precipitation in the water column. At first glance, Fe enrichments in shallower waters and their absence in deeper waters of the White Mfolozi Inlier may appear contradictory, since Fe enrichments are commonly taken to denote water-column anoxia (35). However, our data are entirely consistent with the current understanding of how Fe enrichment may be enhanced under anoxic ferruginous conditions, whereby one prominent pathway for developing high FeHR/FeT and Fe/Al ratios is via upwelling of deep, anoxic waters into shallower oxic settings (35, 36).

After Mn and Fe (oxyhydr)oxides had formed and been deposited, they were then largely converted to carbonate minerals through microbial respiration during diagenesis, as indicated by high Fe_{carb} concentrations in sediments of sequences I and II (*SI Appendix*, Table S1). In support of this, highly negative $\delta^{13}C$ values [between −22‰ and −13‰, Vienna Pee Dee Belemnite (VPDB) and $\delta^{18}O$ values (between −21‰ and −8‰, VPDB] indicate carbonate precipitation through organic carbon (OC) remineralization during diagenesis (7, 37). This happened below the sediment–water interface in sediments deposited under a water column characterized by relatively high rates of OC burial (high productivity) (7). In contrast, Fe_{carb} is scarce in the deeper-water sequence III and the more distal Nongoma setting (*SI Appendix*, Table S1), where instead, most of the Fe is associated with chlorite and stilpnomelane (7). It is thus likely that Fe (oxyhydr) oxides were converted to Fe-rich clay minerals during diagenesis in this setting, probably via reverse weathering (38). Another possibility involves conversion of Fe (oxyhydr)oxides into mixed ferrous/ferric phases, such as green rust during settling (39, 40), before their final transformation to stilpnomelane and chlorite during diagenesis and metamorphism. Thermodynamic estimates based on the chemical composition of Fe-chlorite showed that Fe- and Mn-rich clay minerals of the Mozaan Group formed during diagenesis and metamorphism (37). Regardless of the precise nature of precursor Fe minerals, Fe/Al ratios much higher than those in average Pongola shales (ref. 33 and *SI Appendix*, Table S1) indicate that their precipitation gave rise to significant Fe enrichments in the deep-water sediments and during upwelling of deep ferruginous waters into shallower oxic settings.

The $\delta^{13}C_{org}$ values average −27.6‰ in the shallow-water sequence I samples, reflecting isotopic fractionations expected during autotrophic CO_2 fixation (41). During deposition of sequence II, $\delta^{13}C_{org}$ values progressively decrease to the average value of −30‰, and down to −38‰ in the deep-water settings of the White Mfolozi Inlier and Nongoma areas (Fig. 1). The highly negative $\delta^{13}C_{org}$ values in these deeper-water, ferruginous settings likely reflect biological carbon cycling with a significant contribution from methanogens and methanotrophs (42). The variability in biological processes with water-depth might be linked to the water-column redox gradient, where (*i*) high Mn/Fe ratios and Mn(II) oxidation (which requires free O_2) are consistent with

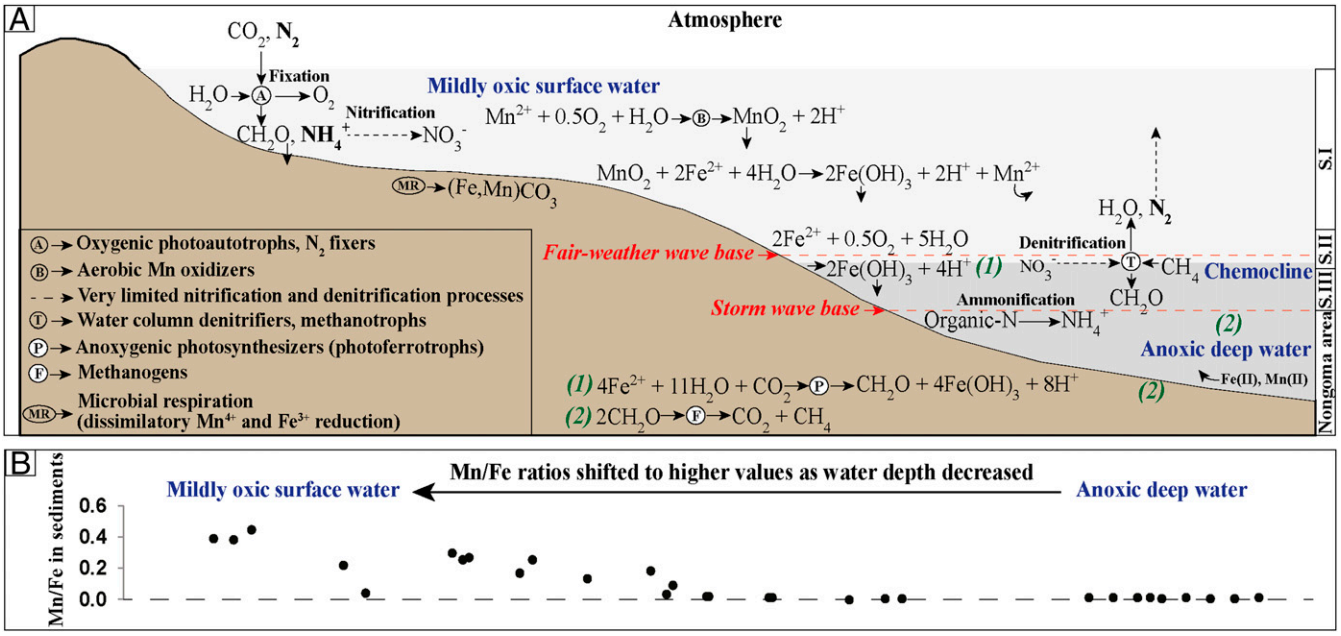

Fig. 2. Proposed paleoenvironmental reconstruction of the Mesoarchean Pongola basin during deposition of the Ntombe Formation, Mozaan Group. (*A*) Water-column chemistry and biogeochemical cycles developed in the localized oxygenated surface waters (recorded by the sequences I and II), overlying anoxic deep waters (recorded by the sequence III and the sedimentary succession in the Nongoma area). Low biological O_2 production in shallow-marine environments likely limited expression of nitrification and denitrification signals in sediments deposited in the Pongola basin. (*B*) Mn/Fe ratios in sediments reflective of seawater redox increase toward the shoreline as ferruginous waters upwelled from anoxic, deep settings to mildly oxygenated, shallow-marine environments. S.I (sequence I); S.II (sequence II); S.III (sequence III). Modified from ref. 7.

photoautotrophic CO_2 fixation and oxygenic photosynthesis in the shallow-water settings, and (*ii*) Fe enrichments without Mn(II) oxidation (Mn/Fe ratios lower than the average Pongola shale values) are consistent with methanotrophs utilizing dissolved O_2 or Fe(III) compounds to oxidize methane at the redoxcline or chemocline, respectively, under hypoxic or anoxic conditions in deeper-water settings. In view of this, the water column appears to have been both redox and ecologically stratified.

N Isotope Systematics and Preservation of Primary Isotopic Signals. Our geochemical data suggest a shallow-water oxygen oasis in the Mesoarchean Pongola sea at ∼2.9 Ga. If these conditions were stable and extensive enough to support oxic nitrogen metabolism, then this should be reflected in nitrogen isotope systematics, as observed in younger Neoarchean sedimentary successions (5, 15, 17, 18, 25). Large N isotope heterogeneity revealed by the NanoSIMS technique in isolated microfossils from the ∼3.0-Ga Farrel Quartzite (Western Australia) has been linked to biological aerobic nitrification (43), indicating the emergence of this metabolic pathway even before deposition of the Mozaan Group. In ancient marine sediments, $\delta^{15}N$ values between −4‰ and +2‰ (Air-N_2) are usually attributed to isotopic fractionation imparted during biological N_2 fixation using the Mo-nitrogenase enzyme (5, 15–18, 25). The use of vanadium-based and Fe-based alternative nitrogenase enzymes produces more depleted $\delta^{15}N$ values, between −6‰ and −8‰ (15, 44). $\delta^{15}N$ values above +4‰ would provide compelling evidence for an aerobic N cycle coupling nitrification and denitrification/anaerobic ammonium oxidation (anammox) processes (e.g., refs. 5, 15, 17, 18, and 25). Nitrogen isotope values for 18 of 22 samples fall in the range of −5 to +3‰ (Air-N_2), and reflect isotopic fractionation driven by Mo-based diazotrophy (Fig. 1 and *SI Appendix*, Table S2). Positive values above +4‰ are limited to four samples, including two from the White Mfolozi Inlier and two others from the more distal Nongoma area.

Here, we exclude abiotic sources for bioavailable nitrogen, because they were probably too small in magnitude and should have otherwise dominated the early Precambrian $\delta^{15}N$ record, counter to what is observed (15). However, several mechanisms can alter the original $\delta^{15}N$ values of marine biomass, ranging from early diagenesis to the thermal degradation of organic matter (OM) during deeper burial diagenesis and metamorphism (15, 45–48). The redox state of the water column, sedimentation rate, and OM accumulation can also impart different N isotope fractionations between sinking organic particles and surficial marine sediments. NH_4^+ release during OM remineralization below the sediment–water interface and partial oxidation in pore waters can increase bulk sediment $\delta^{15}N$ ($\delta^{15}N_{bulk}$) values by ∼4‰ under oxic diagenetic conditions, while this effect tends to be minimal during anoxic diagenesis, with an isotopic fractionation <1‰ (15, 45). The predominance of Fe and Mn carbonate minerals derived from the reduction of Fe and Mn (oxyhydr)oxides indicates anoxic diagenetic conditions (7, 37) and thus likely a minimal effect of early diagenetic processes on primary $\delta^{15}N$ values. Importantly, oxic diagenesis would result in isotopic compositions that reflect an aerobic nitrogen cycle, which is not seen in our dataset.

Organic-bound NH_4^+ can also be released through thermal devolatization of OM during burial diagenesis and metamorphism, resulting in a maximum increase in $\delta^{15}N_{bulk}$ values of 1 to 2‰ at greenschist facies, 3 to 4‰ at lower amphibolite facies, and up to 6 to 12‰ at upper amphibolite facies; even larger offsets can occur in sedimentary rocks affected by circulating fluids (46). The Mozaan Group experienced lower greenschist facies metamorphism (37), suggesting a maximum increase in $\delta^{15}N_{bulk}$ values of less than 2‰. To alleviate potential effects caused by mechanisms described above on $\delta^{15}N$ values, N isotope data were also measured on extracted kerogen ($\delta^{15}N_{ker}$) to compare with bulk sample data ($\delta^{15}N_{bulk}$). The offset between $\delta^{15}N_{bulk}$ and $\delta^{15}N_{ker}$ values allows evaluation of the extent of preservation of the N isotope signature imparted by the initially deposited biomass. Two samples from the Nongoma area showing evidence for hydrothermal processes are characterized by large offsets between $\delta^{15}N_{bulk}$ and $\delta^{15}N_{ker}$ values and by very positive N isotope values (Fig. 1 and *SI Appendix*, Table S2), which likely support postdepositional alteration by circulating fluids. Therefore, these two samples will not be further considered in this study. In contrast, the minimal offset in most of the studied samples supports good preservation of the primary isotopic signature (Fig. 1 and *SI Appendix*, Table S2). The samples with minimal offset between $\delta^{15}N_{bulk}$ and $\delta^{15}N_{ker}$ values also lack evidence of secondary alteration by later circulating fluids or hydrothermal processes (37). Furthermore, a minimal effect of postdepositional processes on the isotope composition of biomass is also indicated by the absence of covariation between $\delta^{15}N$ and total N (TN), $\delta^{15}N$ and C/N, $\delta^{15}N$ and $\delta^{13}C$, as well as $\delta^{13}C_{TOC}$ and total OC (TOC) for bulk sediments (*SI Appendix*, Fig. S4). A weak negative covariation between $\Delta^{15}N_{ker-bulk}$ (the difference between $\delta^{15}N_{ker}$ and $\delta^{15}N_{bulk}$) and total K further supports a minimal contribution of ammoniated phyllosilicates (e.g., NH_4^+ substituted for K^+) with a distinct isotopic composition (*SI Appendix*, Fig. S5).

A Lack of Evidence for Aerobic Nitrogen Cycling in the Mesoarchean Pongola Basin Oxygen Oasis. In the modern ocean, where the main processes intrinsic to the aerobic N cycle (including N_2 fixation, nitrification, and denitrification/anammox) are at play, $\delta^{15}N$ values of +5‰ to +7‰ in sedimentary OM reflect ^{14}N loss to the atmosphere through denitrification and anammox in oxygen-minimum zones (48). Buried biomass is an indirect archive of this process, because organisms assimilate the isotopically heavy nitrate (NO_3^-) as a nutrient. Therefore, $\delta^{15}N$ values of +4‰ or greater found in Neoarchean marine sediments are interpreted to reflect temporary aerobic N cycling (e.g., refs. 5, 15, 17, 18, and 25). In contrast, the nitrogen isotope data of the Mozaan Group are inconsistent with the establishment of a significant aerobic nitrogen cycle. Assuming that Mn(II) oxidation occurs at higher redox potential than NH_4^+ oxidation, redox conditions may have been sufficient for evolved nitrifying bacteria in the Pongola basin, because high Mn concentrations in sequence I indicate the precipitation of Mn(IV) (oxyhydr)oxide minerals (7), which required O_2. Photochemical oxidation of Mn is inhibited under Fe-saturated conditions (49), and, unlike Fe(II), significant oxidation of Mn requires oxygen and a catalyst (50). It is thus likely that free O_2 was locally available in the water column during deposition of sequence I (7) and that the subtle increase in $\delta^{15}N_{ker}$ values (up to +5.2‰) measured in two samples from the upper part of sequence I (deposited at the redoxcline) may reflect nitrification/denitrification and uptake of residual nitrate in the water column (Fig. 2). However, the absence of a more compelling isotopic shift in $\delta^{15}N$ values over the extended stratigraphic interval indicates that NO_3^- (i.e., the residual nitrogen species that carries the isotopic information in the modern ocean) did not build up to high enough concentrations to be an important nitrogen source to the biosphere.

While the iron and manganese proxies have the capacity to promptly respond to redox perturbations on a local scale, the nitrogen isotope proxy requires the buildup of a dissolved nitrogen reservoir that carries the isotopic effects of redox reactions at the ecosystem scale. A good modern analog illustrating such a discrepancy between Mn (higher redox potential) and N (lower redox potential) cycles can be found in the Black Sea. Here, rapid oxygen-dependent microbial Mn(II) oxidation is observed at low micromolar (<3 to 5 μM) dissolved oxygen contents in the suboxic zone of the Black Sea (51), where nitrification produces a maximum nitrate concentration of only 3.5 μM (52). However, this maximum nitrate level appears to be too low to leave an isotopic signature of aerobic N cycling (53) (in contrast to open-ocean nitrate concentrations of up to ∼35 μM, which leave an average $\delta^{15}N$ signal of around +5‰; ref. 15 and references therein). Estimates

of O_2 contents based on δ^{56}Fe variations in Mesoarchean oxygen oases suggest a maximum concentration of 10 μM (7, 11). Such dissolved O_2 levels are thus consistent with the potential activity of both Mn(II) oxidizing and nitrifying bacteria during deposition of the Mozaan Group.

It appears that the geographical extent of oxygen oases was likely too restricted in the Mesoarchean ocean to develop a nitrate reservoir that was large enough to leave an isotopic signature, which contrasts with their Neoarchean equivalents [assuming water-column O_2 concentrations were similar in the Mesoarchean and Neoarchean oxygen oases; (7, 11, 29)]. An overwhelming supply of reducing inputs [e.g., Fe(II) and Mn(II)] from submarine volcanism to the Mesoarchean ocean could have suppressed more widespread oxygenation and, thus, limited nitrification. However, iron formation (IF) secular records (e.g., refs. 54 and 55) indicate that volumetrically, the Neoarchean IFs are much larger than their Mesoarchean analogs, yet the Neoarchean to early Paleoproterozoic IFs are characterized by compelling evidence for aerobic N cycling (5, 25, 56). It therefore appears that the reducing sinks from submarine volcanism were not the main driving factor that suppressed the expression of aerobic N cycle in the Mesoarchean ocean.

Implications for Oxygenic Photosynthesis in the Mesoarchean Ocean. Overall, our data reveal an ecosystem that was dominated by Mo-based diazotrophy in an oxygen oasis where a combination of the restricted spatial extent and low dissolved O_2 concentration likely limited the buildup of a sufficient nitrate reservoir to impart an isotopic expression of aerobic N cycling. In the modern ocean, cyanobacteria are the main N_2 fixers (57), and our data suggest that this relationship may extend back to the Mesoarchean. Mo-based diazotrophy requires soluble MoO_4^{2-} availability in the ocean. In the modern ocean, Mo is mainly delivered via riverine inputs after oxidative continental weathering, with a minor contribution from submarine hydrothermal systems (see ref. 16 and references therein). The mild Mo enrichment (relative to average concentration for the upper crust) recorded by the Mozaan Group (*SI Appendix*, Table S1) suggests that dissolved Mo was available in this oxygen oasis (8). However, it has been shown that a very low Mo content (down to 1 nM, which is around 1% of modern seawater concentrations) can sustain Mo-based diazotrophy in modern environments (58). In view of this, submarine hydrothermal Mo inputs could have been sufficient to sustain Mo-based N_2 fixation in the Archean ocean (see ref. 16 and references therein). Moreover, it has also been demonstrated that continental Mo could have been mobilized and delivered to the ocean, even under Archean anoxic atmospheric conditions (O_2 concentration $<10^{-5}$ present atmospheric level; refs. 59 and 60 and references therein).

Free O_2 produced by oxygenic photosynthesis had an impact on the water-column redox and ecological gradients of the Pongola basin, as observed in stable-isotope data confirming aerobic Fe and Mn cycling in shallow-water settings (7). Bioavailable N and P are the main nutrients that control marine productivity over time (e.g., refs. 19–23). Their scarcity may have limited biological O_2 production, resulting in delayed pervasive and permanent oxygenation of the atmosphere–hydrosphere system after the emergence of oxygenic photosynthesis in the Mesoarchean. Since our δ^{15}N data indicate that N was bioavailable in the Mesoarchean marine oasis, P scarcity could have been the main limiting factor in biological O_2 production, consistent with previous biogeochemical modeling (29). Indeed, we observe very low P contents in the Pongola sediments (Fig. 1 and *SI Appendix*, Table S1), which would be entirely consistent with the suggestion of widespread P limitation under global ferruginous conditions (21) and before more extensive anoxic P recycling linked to the buildup of seawater sulfate following more expansive environmental oxygenation (22).

It is possible that positive δ^{15}N values in the ∼3.2-Ga riverine deposits of the Moodies Group, South Africa [interpreted as evidence for denitrification (12)] and a weakly oxidizing U cycle in the Mesoarchean ocean (11, 61) may reflect episodes of mild, local oxidizing conditions in the atmosphere–hydrosphere system (ref. 13 and references therein). However, estimates based on preserved Mesoarchean detrital uraninite in the Witwatersrand Supergroup, South Africa, deposited contemporaneously with the Pongola Supergroup, suggest that atmospheric O_2 concentrations were lower than 3.2×10^{-5} atm (62). Furthermore, the general absence of δ^{15}N values above +4‰ in most Mesoarchean marine and continental deposits around the world (refs. 15, 16, and 63 and this study) is consistent with the view that low rates of biological O_2 production limited the geographical extent of oases and, ultimately, controlled the size of the seawater nitrate reservoir, which did not reach the level necessary to leave a more widespread and persistent isotopic signature of an aerobic N cycle. Regardless of the mechanism(s) that controlled dissolved P concentrations in Archean oceans, oxygenation of Earth's early biosphere was apparently limited by a low supply of bioavailable P, rather than N, under anoxic to very low oxygen surface conditions.

Methods

Major and Trace Elements. Powdered samples were analyzed for major element concentrations by X-ray fluorescence spectroscopy on fusion beads, using a PANalytical MagiX Pro PW2540 spectrometer at the University of Johannesburg. Accuracy was checked with certified reference materials and was better than 1%. Elemental concentrations are reported in wt %, with a detection limit of 0.04 wt %. Trace elements were measured at the University of Tuebingen according to the analytical procedure previously described (14, 64). Analyses were performed using the iCap-Qc ICP-MS instrument coupled to an ESI SC-2 DX autosampler with an ESI Fast uptake system equipped with a 4-mL sample loop. Analytical accuracy, estimated from the 1 relative SD of the mean, varied between 3% and 15% and was monitored by repeated measurements of reference materials OU-6, QS-1, W-2a, and AGV-2 (see *SI Appendix* for analytical details). Enrichment factors were calculated as $(\text{element/Al})_{\text{sample}}/(\text{element/Al})_{\text{reference}}$ using the average concentrations for the upper crust as reference (65).

Iron Speciation Analysis. Iron speciation analysis was performed at the University of Leeds using a calibrated sequential extraction protocol followed by Fe analysis via atomic absorption spectroscopy (66). This method is designed to quantify four different pools of Fe considered to be highly reactive (FeHR) toward H_2S in surface and near-surface environments: (*i*) pyrite S extracted via Cr reduction, followed by trapping as Ag_2S, with Fe calculated assuming an FeS_2 stoichiometry (Fe_{Py}); (*ii*) carbonate-associated iron extracted with a sodium acetate solution (Fe_{Carb}); (*iii*) ferric oxides extracted with a dithionite solution (Fe_{Ox}); and (*iv*) mixed-valence iron oxides, principally magnetite, extracted using ammonium oxalate (Fe_{Mag}) (see *SI Appendix* for further description).

Carbon and Nitrogen Isotope Analyses. The nitrogen isotope composition of bulk rock ($\delta^{15}N_{bulk}$) and the carbon and nitrogen isotope compositions of the extracted kerogen ($\delta^{13}C_{org}$, $\delta^{15}N_{ker}$) were determined by elemental analysis/isotope ratio mass spectrometry at the Institute of Earth Surface Dynamics of University of Lausanne, using a Carlo Erba 1108 (Fisons Instruments) elemental analyzer connected to a Delta V Plus isotope ratio mass spectrometer via a ConFlo III open-split interface (both of Thermo Fisher Scientific) operated under continuous helium flow (67, 68). The average δ^{13}C value obtained for the reference material USGS40 was −26.4 ± 0.1‰ ($n = 6$), which is in good agreement with accepted value of −26.39‰ (69). The accuracy of the analyses was checked periodically through the analysis of international reference materials. For δ^{15}N, we obtained −4.5 ± 0.2‰ ($n = 6$) for USGS40 and +1.0 ± 0.2‰ for IAEA-600, also in good agreement with accepted values of −4.52‰ and +1.0‰, respectively (69). TOC and TN concentrations were determined from the peak areas of the major isotopes using the calibrations for δ^{13}C and δ^{15}N values. The repeatability was better than 0.2 wt % for carbon and nitrogen contents (see *SI Appendix* for further description).

ACKNOWLEDGMENTS. A.H. thanks Anglo Gold Ashanti, Acclaim Exploration NL, J. Hancox, and N. Hicks for access to drill core samples. J.E.S. thanks T. Adatte for X-ray diffraction analysis. We thank the editor for careful handling of our manuscript and Kurt Konhauser and an anonymous reviewer for their meaningful comments that significantly improved the manuscript. This study was funded by the University of Johannesburg; the National Research Foundation of South Africa [Department of Science and Technology Innovation

Research Fellowship (F.O.O.), Grant 75892 (to A.H.), and the Centre of Excellence for Integrated Mineral and Energy Resource Analysis hosted by the University of Johannesburg]; the German Research Foundation Grant SCHO1071/7-1 under the DFG Priority Programme SPP 1833 "Building a Habitable Earth" (to R.S.); and the University of Lausanne. S.W.P. acknowledges support from a Royal Society Wolfson Research Merit Award and a Leverhulme Research Fellowship. A.B. acknowledges support from the Natural Sciences and Engineering Research Council of Canada Discovery and Accelerator grants.

1. Bekker A, et al. (2004) Dating the rise of atmospheric oxygen. *Nature* 427:117–120.
2. Farquhar J, Bao H, Thiemens M (2000) Atmospheric influence of Earth's earliest sulfur cycle. *Science* 289:756–759.
3. Kasting JF, Siefert JL (2002) Life and the evolution of Earth's atmosphere. *Science* 296: 1066–1068.
4. Anbar AD, et al. (2007) A whiff of oxygen before the great oxidation event? *Science* 317:1903–1906.
5. Garvin J, Buick R, Anbar AD, Arnold GL, Kaufman AJ (2009) Isotopic evidence for an aerobic nitrogen cycle in the latest Archean. *Science* 323:1045–1048.
6. Wille M, et al. (2007) Evidence for a gradual rise of oxygen between 2.6 and 2.5 Ga from Mo isotopes and Re-PGE signatures in shales. *Geochim Cosmochim Acta* 71:2417–2435.
7. Ossa Ossa F, et al. (2018) Aerobic iron and manganese cycling in a redox-stratified Mesoarchean epicontinental sea. *Earth Planet Sci Lett* 500:28–40.
8. Planavsky NJ, et al. (2014) Evidence for oxygenic photosynthesis half a billion years before the Great Oxidation Event. *Nat Geosci* 7:283–286.
9. Eickmann B, et al. (2018) Isotopic evidence for oxygenated Mesoarchaean shallow oceans. *Nat Geosci* 11:133–138.
10. Albut G, et al. (2018) Modern rather than Mesoarchaean oxidative weathering responsible for the heavy stable Cr isotopic signatures of the 2.95 Ga old Ijzermijn iron formation (South Africa). *Geochim Cosmochim Acta* 228:157–189.
11. Satkoski A, Beukes NJ, Li W, Beard BL, Johnson CM (2015) A redox-stratified ocean 3.2 billion years ago. *Earth Planet Sci Lett* 430:43–53.
12. Homann M, et al. (2018) Microbial life and biogeochemical cycling on land 3,220 million years ago. *Nat Geosci* 11:665–671.
13. Lyons TW, Reinhard CT, Planavsky NJ (2014) The rise of oxygen in Earth's early ocean and atmosphere. *Nature* 506:307–315.
14. Kurzweil F, Wille M, Gantert N, Beukes NJ, Schoenberg R (2018) Manganese oxide shuttling in pre-GOE oceans–Evidence from molybdenum and iron isotopes. *Earth Planet Sci Lett* 452:69–78.
15. Stüeken EE, Kipp MA, Koehler MC, Buick R (2016) The evolution of Earth's biogeochemical nitrogen cycle. *Earth Sci Rev* 160:220–239.
16. Stüeken EE, Buick R, Guy BM, Koehler MC (2015) Isotopic evidence for biological nitrogen fixation by molybdenum-nitrogenase from 3.2 Gyr. *Nature* 520:666–669.
17. Berman-Frank I, Lundgren P, Falkowski P (2003) Nitrogen fixation and photosynthetic oxygen evolution in cyanobacteria. *Res Microbiol* 154:157–164.
18. Koehler MC, Buick R, Kipp MA, Stüeken EE, Zaloumis J (2018) Transient surface ocean oxygenation recorded in the ∼2.66-Ga Jeerinah Formation, Australia. *Proc Natl Acad Sci USA* 115:7711–7716.
19. Falkowski PG (1997) Evolution of the nitrogen cycle and its influence on the biological sequestration of CO2 in the ocean. *Nature* 387:272–275.
20. Tyrrell T (1999) The relative influences of nitrogen and phosphorus on oceanic primary production. *Nature* 400:525–531.
21. Reinhard CT, et al. (2017) Evolution of the global phosphorus cycle. *Nature* 541:386–389.
22. Poulton SW (2017) Early phosphorus redigested. *Nat Geosci* 10:75–76.
23. Kipp MA, Stüeken EE (2017) Biomass recycling and Earth's early phosphorus cycle. *Sci Adv* 3:eaao4795.
24. Luo G, et al. (2018) Nitrogen fixation sustained productivity in the wake of the Palaeoproterozoic Great Oxygenation Event. *Nat Commun* 9:978.
25. Godfrey LV, Falkowski PG (2009) The cycling and redox state of nitrogen in the Archaean ocean. *Nat Geosci* 2:725–729.
26. Cardona T, Sánchez-Baracaldo P, Rutherford AW, Larkum AW (2018) Early Archean origin of Photosystem II. *Geobiology* 17:127–150.
27. Magnabosco C, Moore KR, Wolfe JM, Fournier GP (2018) Dating phototrophic microbial lineages with reticulate gene histories. *Geobiology* 16:179–189.
28. Shih PM, Hemp J, Ward LM, Matzke NJ, Fischer WW (2017) Crown group Oxyphotobacteria postdate the rise of oxygen. *Geobiology* 15:19–29.
29. Olson SL, Kump LR, Kasting JF (2013) Quantifying the areal extent and dissolved oxygen concentrations of Archean oxygen oases. *Chem Geol* 362:35–43.
30. Planavsky NJ, et al. (2010) The evolution of the marine phosphate reservoir. *Nature* 467:1088–1090.
31. Bjerrum CJ, Canfield DE (2002) Ocean productivity before about 1.9 Gyr ago limited by phosphorus adsorption onto iron oxides. *Nature* 417:159–162.
32. Konhauser KO, Lalonde SV, Amskold L, Holland HD (2007) Was there really an Archean phosphate crisis? *Science* 315:1234.
33. Wronkiewicz DJ, Condie KC (1989) Geochemistry and provenance of sediments from the Pongola Supergroup, South Africa; evidence for a 3.0-Ga-old continental craton. *Geochim Cosmochim Acta* 53:1537–1549.
34. Kappler A, Pasquero C, Konhauser KO, Newman DK (2005) Deposition of banded iron formations by anoxygenic phototrophic Fe(II)-oxidizing bacteria. *Geology* 33:865–868.
35. Poulton SW, Canfield DE (2011) Ferruginous conditions: A dominant feature of the ocean through Earth's history. *Elements* 7:107–112.
36. Zhang K, et al. (2018) Oxygenation of the Mesoproterozoic ocean and the evolution of complex eukaryotes. *Nat Geosci* 11:345–350.
37. Ossa Ossa F, et al. (2016) Unusual manganese enrichment in the Mesoarchean Mozaan Group, Pongola Supergroup, South Africa. *Precambrian Res* 281:414–433.
38. Isson TT, Planavsky NJ (2018) Reverse weathering as a long-term stabilizer of marine pH and planetary climate. *Nature* 560:471–475.
39. Zegeye A, et al. (2012) Green rust formation controls nutrient availability in a ferruginous water column. *Geology* 40:599–602.
40. Halevy I, et al. (2017) A key role for green rust in the Precambrian oceans and the genesis of iron formations. *Nat Geosci* 10:135–139.
41. Fogel ML, Cifuentes LA (1993) Isotope fractionation during primary production. *Organic Geochemistry*, eds Engel MH, Macko SA (Plenum, New York), pp 73–98.
42. Stüeken EE, et al. (2017) Environmental niches and metabolic diversity in Neoarchean lakes. *Geobiology* 15:767–783.
43. Delarue F, et al. (2018) Nitrogen isotope signatures of microfossils suggest aerobic metabolism 3.0 Gyr ago. *Geochem Perspect Lett* 7:32–36.
44. Zhang X, Sigman DM, Morel FM, Kraepiel AM (2014) Nitrogen isotope fractionation by alternative nitrogenases and past ocean anoxia. *Proc Natl Acad Sci USA* 111:4782–4787.
45. Lehman MR, Bernasconi SM, Barbieri A, McKenzie JA (2002) Preservation of organic matter and alteration of its carbon and nitrogen isotope composition during simulated and in situ early sedimentary diagenesis. *Geochim Cosmochim Acta* 66:3573–3584.
46. Ader M, et al. (2006) Nitrogen isotopic evolution of carbonaceous matter during metamorphism: Methodology and preliminary results. *Chem Geol* 232:152–169.
47. Ader M, et al. (2016) Interpretation of the nitrogen isotopic composition of Precambrian sedimentary rocks: Assumptions and perspectives. *Chem Geol* 429:93–110.
48. Lam P, Kuypers MM (2011) Microbial nitrogen cycling processes in oxygen minimum zones. *Annu Rev Mar Sci* 3:317–345.
49. Anbar AD, Holland HD (1992) The photochemistry of manganese and the origin of banded iron formations. *Geochim Cosmochim Acta* 56:2595–2603.
50. Tebo BM, Johnson HA, McCarthy JK, Templeton AS (2005) Geomicrobiology of manganese(II) oxidation. *Trends Microbiol* 13:421–428.
51. Clement BG, Luther GW, III, Tebo BM (2009) Rapid, oxygen-dependent microbial Mn(II) oxidation kinetics at sub-micromolar oxygen concentrations in the Black Sea suboxic zone. *Geochim Cosmochim Acta* 73:1878–1889.
52. Fuchsman CA, Murray JW, Konovalov SK (2008) Concentration and natural stable isotope profiles of nitrogen species in the Black Sea. *Mar Chem* 111:90–105.
53. Fulton JM, Arthur MA, Freeman KH (2012) Black Sea nitrogen cycling and the preservation of phytoplankton δ^{15}N signals during the Holocene. *Global Biogeochem Cycles* 26:GB2030.
54. Bekker A, et al. (2014) Iron formations: Their origins and implications for ancient seawater chemistry. *Treatise on Geochemistry*, eds Holland HD, Turekian KK (Elsevier, Oxford), 2nd Ed, Vol 9, pp 561–628.
55. Konhauser KO, et al. (2017) Iron formations: A global record of neoarchaean to palaeoproterozoic environmental history. *Earth Sci Rev* 172:140–177.
56. Busigny V, Lebeau O, Ader M, Krapež B, Bekker A (2013) Nitrogen cycle in the Late Archean ferruginous ocean. *Chem Geol* 362:115–130.
57. Capone DG, Zehr JP, Paerl HW, Bergman B, Carpenter EJ (1997) Trichodesmium, a globally significant marine cyanobacterium. *Science* 276:1221–1229.
58. Glass JB, Wolfe-Simon F, Elser JJ, Anbar AD (2010) Molybdenum–nitrogen colimitation in freshwater and coastal heterocystous cyanobacteria. *Limnol Oceanogr* 55:667–676.
59. Sverjensky DA, Lee N (2010) The great oxidation event and mineral diversification. *Elements* 6:31–36.
60. Lalonde SV, Konhauser KO (2015) Benthic perspective on Earth's oldest evidence for oxygenic photosynthesis. *Proc Natl Acad Sci USA* 112:995–1000.
61. Wang X, et al. (2018) A Mesoarchean shift in uranium isotope systematics. *Geochim Cosmochim Acta* 238:438–452.
62. Burron I, et al. (2018) 3.2 Ga detrital uraninite in the Witwatersrand Basin, South Africa: Evidence of a reducing Archean atmosphere. *Geology* 46:295–298.
63. Koehler MC, Buick R, Barley ME (2018) Nitrogen isotope evidence for anoxic deep marine environments from the Mesoarchean Mosquito Creek Formation, Australia. *Precambrian Res* 320:281–290.
64. Babechuk MG, Widdowson M, Murphy M, Kamber BS (2015) A combined Y/Ho, high field strength element (HFSE) and Nd isotope perspective on basalt weathering, Deccan Traps, India. *Chem Geol* 396:25–41.
65. Taylor S, McLennan S (1985) *The Continental Crust: Its Evolution and Composition* (Blackwell, London).
66. Poulton SW, Canfield DE (2005) Development of a sequential extraction procedure for iron: Implications for iron partitioning in continentally derived particulates. *Chem Geol* 214:209–221.
67. Spangenberg JE, Jacomet S, Schibler J (2006) Chemical analyses of organic residues in archaeological pottery from Arbon Bleiche 3, Switzerland—Evidence for dairying in the late Neolithic. *J Archaeol Sci* 33:1–13.
68. Spangenberg JE, Bagnoud-Velásquez M, Boggiani PC, Gaucher C (2014) Redox variations and bioproductivity in the ediacaran: Evidence from inorganic and organic geochemistry of the corumbá group, Brazil. *Gondwana Res* 26:1186–1207.
69. Brand WA, Coplen TB, Vogl J, Rosner M, Prohaska T (2014) Assessment of international reference materials for isotope-ratio analysis (IUPAC Technical Report). *Pure Appl Chem* 86:425–467.
70. Clarkson MO, Poulton SW, Guilbaud R, Wood RA (2014) Assessing the utility of Fe/Al and Fe-speciation to record water column redox conditions in carbonate-rich sediments. *Chem Geol* 382:111–122.